

Tectonically controlled, time-predictable basaltic volcanism from a lithospheric mantle source (central Basin and Range Province, USA)

Greg A. Valentine*, Frank V. Perry

Mail Stop D462, Earth and Environmental Sciences Division, Los Alamos National Laboratory, Los Alamos, NM 87545 USA

Received 9 March 2007; received in revised form 22 June 2007; accepted 22 June 2007

Available online 2 August 2007

Editor: R.W. Carlson

Abstract

Understanding the evolution of basaltic volcanic fields is critical to our concepts of basaltic magmatism and to volcanic risk assessment. We summarize physical volcanological, geochemical, and time–volume characteristics of the Plio-Pleistocene part of the Southwestern Nevada Volcanic Field (SNVF) as an example of an extremely low volume-flux end member of basaltic fields. The SNVF has produced 17 volcanoes of dominantly trachybasaltic composition over the past 5 Myr with a total volume of slightly less than 6 km^3 . Eruptive fissure lengths, volumes, and inferred lava effusion rates decreased between Pliocene- and Pleistocene-age volcanoes. Major element data suggest that most of the magmas underwent similar degrees of fractionation during ascent, and trace element compositions indicate a decrease in the degree of partial melting of the lithospheric mantle source since $\sim 3 \text{ Ma}$. Isotopic data support an interpretation wherein magmas ascended relatively quickly from their source regions with little if any interaction with crustal rocks. Relationships between age and cumulative erupted volume indicate that the repose interval between eruptive episodes is determined by the volumes of prior episodes and, since $\sim 3 \text{ Ma}$, an average eruption rate of $\sim 0.5 \text{ km}^3/\text{Myr}$, i.e., the field is time-predictable. All of these features support a model wherein magmatism is a passive result of regional tectonic strain. Partial melt resides in pockets of lithospheric mantle that are relatively enriched in hydrous minerals; slow deformation focuses melt, occasionally resulting in sufficiently high melt pressure to drive dikes upward and feed eruptive episodes. Larger source volumes result in larger eruptive volumes and wider dikes that relieve relatively more strain in the crust than smaller volume events, and therefore are followed by longer repose intervals required for recovery of crustal stresses. We suggest that time-predictability may be a fundamental property of tectonically controlled basaltic fields, where melt accumulation and ascent are controlled by tectonic strain rate. This behavior contrasts with magmatically controlled fields where magma flux is sufficiently high to overwhelm local tectonic strain, eruptions are primarily caused by magmatic processes that build pressure in reservoirs, and the systems are more likely to be volume-predictable.

© 2007 Elsevier B.V. All rights reserved.

Keywords: basaltic field; lithospheric mantle; dike; effusion rate; time-predictable; volume-predictable

1. Introduction

Monogenetic basaltic volcanic fields occur in extensional (e.g., Basin and Range Province of North America, and the African-Arabian rift system (Camp et al., 1991; Aranda-Gómez et al., 2003)) or somewhat

* Corresponding author.

E-mail address: gav@lanl.gov (G.A. Valentine).



Fig. 1. Map of southwestern U.S.A. showing the northern, central, and southern parts (NBR, CBR, and SBR, respectively) of the Basin and Range province (after Sonder and Jones, 1999), the location of the Southwest Nevada Volcanic Field, and the area of Fig. 2 (partial rectangular area is the area of Fig. 2 that overlaps SNVF).

neutral tectonic settings (e.g., Colorado Plateau, USA, and Auckland, New Zealand (Condit et al., 1989; Briggs et al., 1994)), as well as in convergent settings (e.g., Trans-Mexican volcanic belt (Connor, 1990)) and associated back-arc areas (e.g., Ojika Jima District, southwest Japan (Sudo et al., 1998)). The fields range from a small number of widely scattered volcanoes with relatively low eruptive volume fluxes (over the lifetime of the field), such as the Plio-Pleistocene part of the Southwestern Nevada Volcanic Field (SNVF) (Crowe, 1986; Perry et al., 1998; Valentine and Perry, 2006) to densely-spaced cones and shields and surrounding lava plains reflecting high volume fluxes such as the Eastern Snake River Plain (ESRP) (Kuntz et al., 1986). From the standpoint of understanding the fundamental controls on timing and location of volcanoes in basaltic fields it is useful to consider end member cases such as SNVF and ESRP. Differences in the behavior of these fields provide insight into the integrated processes of melt

generation and accumulation in the mantle, ascent through the crust, and interaction of magmas with pre-existing structure in the shallow crust and with topography. In addition to elucidating our overall understanding of basaltic magmatism, such studies can provide key information for volcanic risk to urbanized areas, infrastructure, and long-term facilities that reside within basaltic fields.

This paper focuses on the most recent 5 Myr history of the SNVF (central Basin and Range Province, U.S.A.; Figs. 1,2) as an end member example of a basaltic field with extremely low eruptive volume flux. Basaltic volcanism in the field occurred in six episodes of activity during this period (Perry et al., 1998; Fleck et al., 1996; Connor et al., 2000; Valentine and Perry, 2006). We describe physical volcanological data that provide insight into the length scales of sources tapped for each volcano, the lengths of feeder dikes that transport magmas to the surface, and the relationship

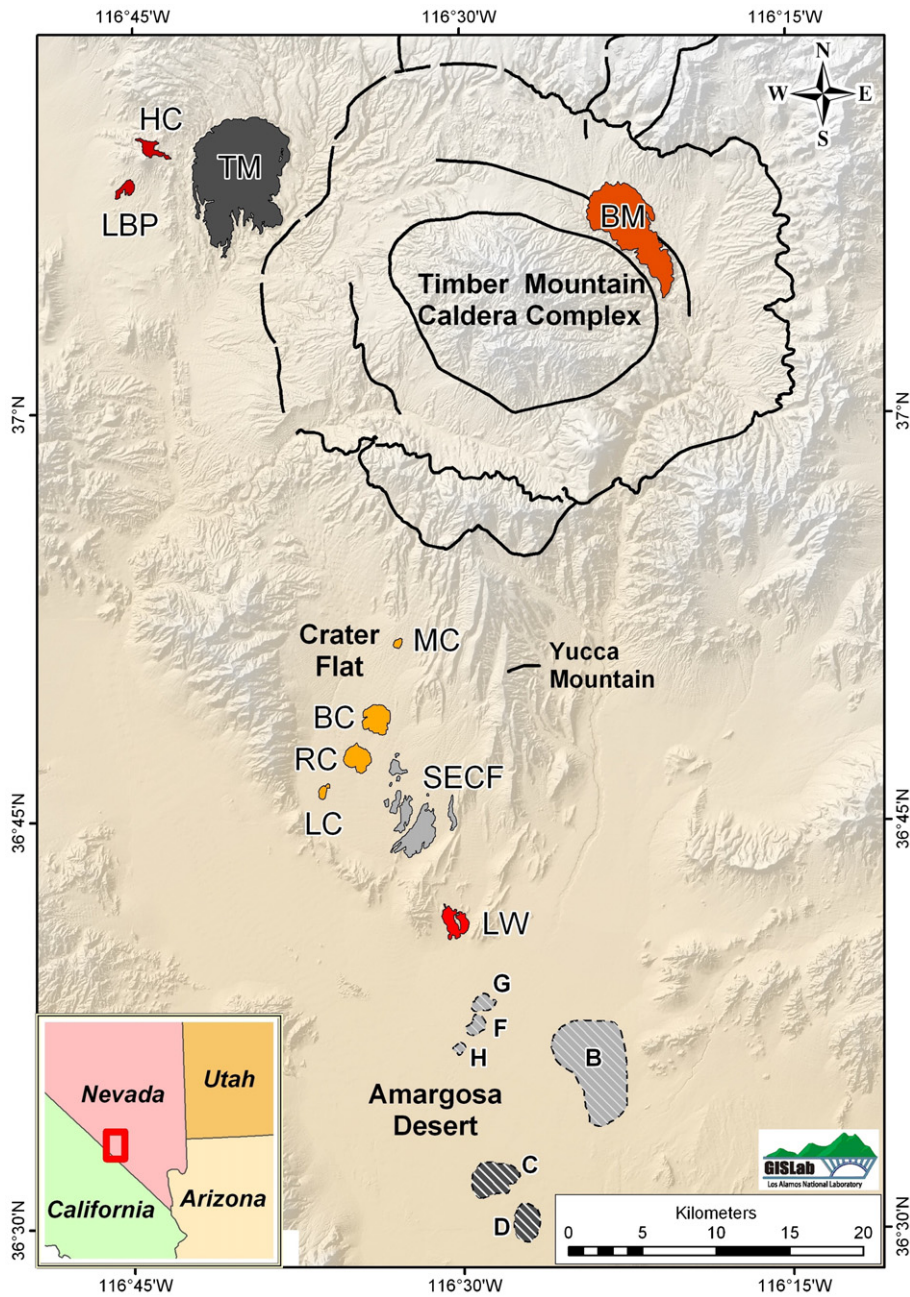


Fig. 2. Shaded relief map of the southwestern part of the Southwest Nevada Volcanic Field showing Plio-Pleistocene volcanoes (buried volcanoes in the southern part of the map area indicated with white diagonal line patterns). Color patterns indicate basalts <3 Ma and gray scale patterns indicate basalts >3 Ma. 4.6 Ma episode — Thirsty Mountain (TM) and Anomalies C and D. 3.8 Ma episode — SE Crater Flat (SECF) and Anomalies B, F, G, and H. 2.9 Ma episode — Buckboard Mesa (BM). 1.1 Ma episode — Makani volcano (MC), Black Cone (BC), Red Cone (RC) and NE and SW Little Cones (LC). 350 ka episode — Little Black Peak (LBP) and Hidden Cone (HC). 77 ka episode — Lathrop Wells volcano (LW). Crater Flat and Amargosa Desert are major basins that host many of the Plio-Pleistocene basalts. Black lines are Miocene caldera boundaries (Wahl et al., 1997).

between lava effusion rates, dike lengths, and volumes at individual volcanoes. We also review geochemical data supporting a conclusion that the primarily trachy-basaltic magmas erupted during this time frame were

derived from compositionally heterogeneous lithospheric mantle and transited the crust relatively quickly without crustal assimilation or significantly different histories of fractional crystallization. Time–volume

relationships indicate that the most recent four episodes of eruptive activity beginning at 2.9 Ma followed time-predictable behavior (Bacon, 1982); the timing of each episode is a function of the volume of the prior episode and a steady eruptive flux of $\sim 0.5 \text{ km}^3/\text{Myr}$ across the volcanic field. All of the above data support a model wherein magmatism in the SNVF is a passive response to relatively slow regional extension. We compare the low-flux SNVF with the Eastern Snake River Plain as an example of an extremely high flux volcanic field. The two fields define tectonically controlled (SNVF) and magmatically controlled (ESRP) end members, which have fundamentally different time–volume relationships as well as different relationships between shallow dikes and vents and pre-existing structures. Finally, we summarize the implications of time-predictable behavior in the SNVF for risk assessment.

2. Overview of geologic setting, physical volcanology, and geochemistry of the Southwestern Nevada Volcanic Field

2.1. Volcanic history and tectonic setting

The SNVF has been active since Mid-Miocene, beginning with large-scale silicic volcanism and many caldera-forming ignimbrite eruptions (Sawyer et al., 1994). Waning silicic volcanism gave way to sporadic basaltic activity that has continued to the $\sim 77 \text{ ka}$ Lathrop Wells volcano (Crowe, 1986; Vaniman et al., 1982; Fleck et al., 1996; Heizler et al., 1999). During the past $\sim 11 \text{ Myr}$ there has been a long-term waning trend in eruptive volume flux on the scale of the volcanic field (Crowe, 1986; Perry et al., 1998). The exact volumes of Late Miocene basalts are difficult to quantify given the degree of faulting, erosion, and local burial of Miocene products, but the areal extent of lavas from that time indicate that volumes of several km^3 were common for individual volcanic centers (Crowe, 1986). Post-Miocene basalts (the last 5 Myr; Fig. 2) are better preserved, although some are buried in alluvial basins (Perry et al., 2005), and comprise slightly less than 6 km^3 of cumulative erupted volume. These basalts erupted in six episodes with ages of $\sim 4.6 \text{ Ma}$, 3.8 Ma , 2.9 Ma , 1.1 Ma , 350 ka , and 77 ka (Fleck et al., 1996; Perry et al., 1998; Heizler et al., 1999); each episode resulted in the formation of 1–5 monogenetic volcanoes within a time span of a few 10s of kyr (see Table 1). The waning of eruptive volume flux over the time-scale of the volcanic field can be understood in terms of the shutoff of thermal input into the lithosphere after breakdown of subduction and loss of the mantle wedge, followed by

conductive cooling of the lithosphere without further thermal input (Perry et al., 1993).

Basalts of the SNVF lie in a unique region that straddles the boundary between the central and northern Basin and Range (Fig. 1). Volcanism in most areas of the Basin and Range began with melting of lithospheric mantle that transitioned to melting of upwelling asthenospheric mantle once the lithosphere was thinned by extension (Perry et al., 1987, 1988; Leeman and Harry, 1993). However, Nd and Sr isotopes indicate that the western half of the central Basin and Range has retained a lithospheric source enriched in incompatible trace elements to the present time (Farmer et al., 1989; Livaccari and Perry, 1993; DePaolo and Daley, 2000). Extension within the central Basin and Range began about 16 Ma, $\sim 10 \text{ Myr}$ later than the onset of extension in the northern and southern parts of the Basin and Range (Sonder and Jones, 1999). The later onset of extension in the central Basin and Range might have limited asthenospheric upwelling and contributed to the preservation of lithospheric mantle beneath the SNVF (cf. Farmer et al., 1989). As with volcanism, extension and related faulting in the immediate vicinity of the SNVF was episodic and occurred in localized domains (Sawyer et al., 1994), and was most active between $\sim 10\text{--}13 \text{ Ma}$ (e.g., extension rates of $8\text{--}36\% \text{ Myr}^{-1}$ in the Crater Flat area (Fridrich et al., 1999)), followed by relatively low extension rates ($0.1\text{--}0.4\% \text{ Myr}^{-1}$) that continue to the present day in the west–southwestern part of the volcanic field where Plio-Pleistocene basalts reside (Fridrich et al., 1999).

2.2. Physical characteristics of the Plio-Pleistocene volcanoes

The six Plio-Pleistocene episodes produced a total of seventeen volcanoes, eleven of which are exposed on the surface (Fig. 2, Table 1). The three oldest (Pliocene) surface volcanoes (Thirsty Mountain, SE Crater Flat, and Buckboard Mesa) each erupted along a fissure, the lengths of which range between 2.5–5 km. Although it is not possible to determine how much original pyroclastic material has been removed by erosion from these volcanoes, the predominance of lavas, fissure vents, and only very proximal remnants of spatter and agglutinate along fissure vents are all consistent with the volcanoes having been dominated by Hawaiian style eruptions (Valentine and Perry, 2006). Estimated effusion rates of lavas at the Pliocene volcanoes are $\sim 40\text{--}100 \text{ m}^3/\text{s}$ (Valentine and Perry, 2006) based upon the correlation between flow length and effusion rate of Walker (1973).

In contrast, the eight Quaternary volcanoes, with one possible exception (Makani volcano), are each characterized by a single scoria cone that preserves evidence of

Table 1
Characteristics of Pliocene–Pleistocene basaltic episodes in the Southwestern Nevada Volcanic Field

Episode age	Volcanoes	Preserved volume (corrected volume) (km ³)	Fissure length ^a (km)	Maximum lava flow length ^a (km)	Brief description
~4.63 Ma ^b	Thirsty Mountain	2.28–2.63 ^c	5	6	Broad shield volcano consisting of stacked lava flows and a central remnant of pyroclastic (near vent) deposits.
	Anomaly C	0.117 ^d			Small lava field (buried)
	Anomaly D	0.073 ^d			Small lava field (buried)
~3.8 Ma ^c	SE Crater Flat	0.56 ^f	3.6	4	Low shield volcano, now broken by normal faults and partially buried by alluvium, with multiple lavas and pyroclastic vent facies exposed.
	Anomaly B	1.227 ^d			Small shield volcano (buried)?
	Anomaly G	0.028 ^d			Small lava field (buried)
	Anomaly F	0.029 ^d			Small lava field (buried)
	Anomaly H	0.006 ^d			Small lava field (buried)
~2.87 Ma ^g	Buckboard Mesa	0.84 ^c	2.5	7.3	Large lava field with remnant of a main pyroclastic cone in northern part, fissure inferred from ridge of lava and pyroclastics that extends SE from main cone.
~1.1 Ma ^h	Black Cone	0.06 ⁱ (0.14)	0.6	1	Pyroclastic cone remnant preserving Strombolian and violent Strombolian facies, and two lava fields that vented from the base of the cone. ⁱ
	Red Cone	0.06 ⁱ (0.14)	0.5	1.4	Pyroclastic cone remnant preserving Strombolian and violent Strombolian facies, and two lava fields that vented from the base of the cone. ⁱ
	Makani (a.k.a. Northern Cone)	0.002 ⁱ (0.005)	0.4	0.4	Small lava mesa with pyroclastic deposits marking location of short fissure. ⁱ
	SW & NE Little Cones	0.03 ⁱ (0.07)	0.3	1.8	Pyroclastic cone remnants, open to the south, each with single lava field mainly buried by alluvium. ⁱ
~350 ka ^j	Little Black Peak	0.014 ^k (0.03)	0.4	1.3	Pyroclastic cone with lavas that extend from its base. ^k
	Hidden Cone	0.03 ^k (0.07)	0.3	1.6	Pyroclastic cone with 2–3 lava fields that extend from near its base. ^k
~77 ka ^l	Lathrop Wells volcano	0.12 ^m	0.8	1.6	Single pyroclastic cone with two lava flow fields that vented from the base of the cone and remnants of a tephra fallout sheet. ^m

^a Reported for volcanoes exposed on the surface only, from Valentine and Perry (2006).

^b Thirsty Mountain age is mean of Fleck et al. (1996). Model ages of Anomalies C and D based upon depth of burial and sedimentation rate.

^c Volumes of volcanoes on surface calculated by integrating digital elevation data above reconstructed paleosurface (based upon basal contacts of basaltic products where exposed). Volume range for Thirsty Mountain allows for possibility that outlying lava remnants originated at this volcano.

^d Volumes of buried basalts based upon areal extent of each aeromagnetic anomaly (Perry et al., 2005) and basalt thickness obtained from drilling.

^e Composite age of SE Crater Flat (Fleck et al., 1996; Perry et al., 1998) and Anomalies G and B which range from ~3.7–3.9 Ma (R.J. Fleck and F.V. Perry, unpub. data).

^f Products of SE Crater Flat eruptions are partially buried beneath alluvium. Volume estimate includes surface deposits and buried deposits, the latter based upon aeromagnetic and drill core data.

^g Fleck et al. (1996).

^h Consistent with ages of Fleck et al. (1996) with further constraints from paleomagnetic time scale of Cande and Kent (1995).

ⁱ Valentine et al. (2006). Values in parentheses are corrected for erosion of likely tephra fallout deposits based upon similarity to Lathrop Wells volcano.

^j Composite mean of ages from Fleck et al. (1996) and Perry et al. (1998), which ranges from ~320–375 ka.

^k Values in parentheses are corrected for erosion of likely tephra fallout deposits based upon similarity to Lathrop Wells volcano (Valentine and Keating, in press).

^l From Heizler et al. (1999).

^m Details of volume calculations and volcanological characteristics provided in Valentine et al. (2007).

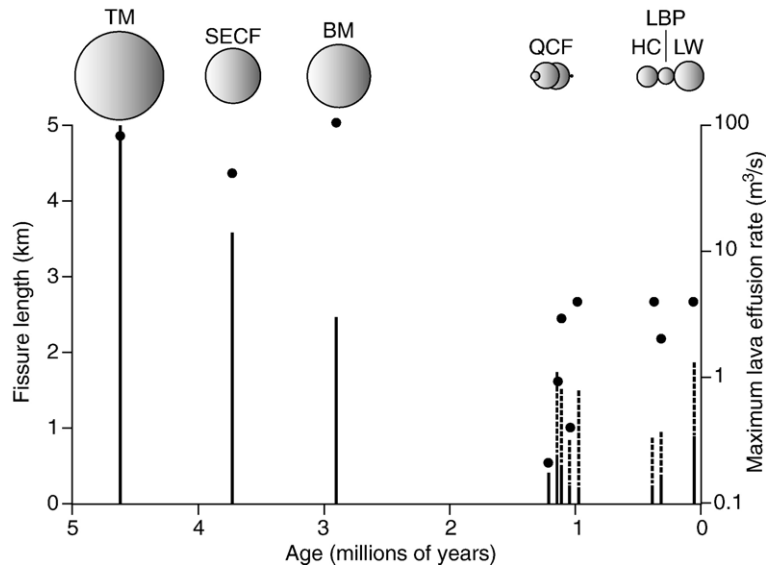


Fig. 3. Plot of preserved eruptive volume (circles sized in proportion to cube-root of volume), fissure length (lines), and estimated effusion rates (dots) for Plio-Pleistocene volcanoes in the Southwestern Nevada Volcanic Field (not including buried volcanoes). Note that age determinations do not allow discrimination of relative ages amongst the volcanoes within the ~ 1.1 Ma episode or within the ~ 350 ka episode, therefore they are plotted in random order around the episode age. Letters TM, SECF, BM, HC, LBP, and LW correspond to volcanoes shown in Fig. 2. QCF refers to all five of the Quaternary volcanoes in Crater Flat (Makani, Black Cone, Red Cone, and SW and NE Little Cones). Modified from Valentine and Perry (2006).

both Strombolian and violent Strombolian activity and by very small lava fields extending 0.4–1.8 km from the vents (estimated effusion rates of ≤ 4 m^3/s) (Valentine et al., 2006, 2007; Valentine and Keating, in press). The youngest volcano (Lathrop Wells, ~ 77 ka) preserves remnants of a tephra fallout deposit that extend ~ 20 km from the cone (Valentine et al., 2007); the estimated ratio of fallout volume to cone plus lava volume is 1.4. Any potential original fallout deposits at the other Quaternary volcanoes are no longer preserved, but the otherwise strong similarity of those volcanoes with Lathrop Wells suggests that they likely had similar proportions of fallout deposits. We infer that each of these volcanoes likely began erupting along a fissure, representing the initial intersection of a feeder dike with the Earth's surface, before eruptive flow focused in to a main conduit (Keating et al., in press). The absence of exposed features that are directly associated with the inferred fissures suggests that maximum initial fissure lengths were no larger than the diameters of the cones (such that the fissures were buried by later pyroclastic deposits); thus the inferred fissure lengths range from ~ 0.3 – 0.8 km.

Fissure lengths, preserved volumes, and estimated effusion rates for the eleven Plio-Pleistocene volcanoes exposed on the surface are summarized in Fig. 3. In an earlier paper (Valentine and Perry, 2006) we suggested that the fissure lengths are proportional to the lengths of

feeder dikes at depth, and that these lengths are in turn closely related to the length scale of the (partially molten) mantle source that is tapped to feed each volcano (simply estimated as the cube root of erupted volume corrected for some reasonable degree of partial melting). Larger erupted volumes reflect larger length scales of tapped sources (magmatic footprints), which in turn are reflected in the feeder dike lengths. However, we did not discuss the physical reasons for correlation between lava effusion rate, fissure (dike) length, and volume; this aspect is returned to Section 4 below.

2.3. Geochemistry of Plio-Pleistocene volcanoes

Plio-Pleistocene volcanic rocks of the SNVF range in composition from basalt to trachybasalt, except for basaltic trachyandesites of the 4.6 Ma and 2.9 Ma episodes (Table 2, Fig. 4(a)). In this paper, we simply refer to all the mafic rocks as basalt. Complete documentation of the geochemical data presented here are found in Perry et al. (1998) and Perry and Straub (1996).

The basalts show considerable variation in major-element composition at similar Mg numbers and MgO content, indicating that mantle melting produced primitive magmas of several compositions (Fig. 4(b)). Mg numbers of basalts generally fall in a narrow range of 53–54 and MgO ranges only between 5–6% (except for basalts of the 3.8 Ma episode in SE Crater Flat,

Table 2
Representative major-element (wt.%), trace-element (ppm) and isotopic compositions of Pliocene–Pleistocene SNVF basalts

Volcanic center	Lathrop Wells (early flow)	Lathrop Wells (late flow)	Hidden Cone	Little Black Peak	Black Cone	Red Cone	Makani Cone	Little Cone SW	Buckboard Mesa	SE Crater Flat	Thirsty Mountain
Sample	LW22FVP	LW41FVP	HC1FVP	LBP2FVP	BC13FVP	RC3FVP	MC7-18-94-1BMC	CF15FVP	BB5FVP	CF12FVP	TM2FVP
SiO ₂	47.43	48.78	48.78	48.15	50.88	50.60	49.07	47.10	53.04	47.69	50.89
TiO ₂	2.06	1.89	1.79	1.88	1.44	1.53	1.61	2.17	1.47	1.86	1.86
Al ₂ O ₃	16.60	16.87	16.87	16.77	17.04	17.26	17.16	16.05	17.59	15.32	17.39
Fe ₂ O ₃	12.15	11.48	11.68	11.77	10.32	10.94	11.01	11.77	8.52	12.28	9.41
MnO	0.18	0.17	0.18	0.17	0.17	0.18	0.17	0.17	0.13	0.18	0.17
MgO	6.13	5.75	5.73	5.63	5.09	5.23	5.20	5.35	4.93	6.56	4.74
CaO	8.40	8.48	9.19	9.37	8.47	8.61	8.70	9.34	6.90	9.36	7.10
Na ₂ O	3.55	3.56	3.44	3.36	3.16	3.27	3.35	3.81	3.92	2.93	4.23
K ₂ O	1.80	1.82	1.64	1.65	1.69	1.87	1.66	2.00	2.37	1.58	2.85
P ₂ O ₅	1.31	1.23	1.10	1.12	0.99	1.10	1.14	1.35	1.02	0.70	0.98
Total	99.60	100.03	100.40	99.87	99.24	100.59	99.06	99.13	99.90	98.45	99.61
Mg# ^a	54.0	53.8	53.3	52.7	53.5	52.7	52.4	51.4	57.4	55.4	54.0
<i>XRF trace-element analyses</i>											
Ba	1315	1374	1313	1369	1508	1530	1405	1450	2208	905	1390
Rb	14	17	16	15	24	20	23	16	34	22	48
Sr	1556	1447	1480	1463	1264	1411	1397	2188	1320	933	949
Y	23	30	37	29	28	37	15	29	20	32	32
Zr	382	374	426	393	379	392	408	428	372	273	371
V	185	184	186	188	149	167	172	196	135	232	167
Cr	106	106	90	76	88	94	66	74	78	180	57
<i>INAA trace-element analyses</i>											
La	92.6	93.9	114.7	104.1	112	114.6	115.8	134.3	84.7	70	70.7
Ce	184	181	204	194.4	198.5	209	213	258	162.1	135.8	142.2
Sm	12.7	12.2	12.6	12.5	11.38	12.31	12.72	16.08	9.49	9.82	10.06
Eu	3.28	3.11	3.18	3.24	2.87	3.12	3.2	3.96	2.57	2.61	2.58
Tb	1.17	1.12	1.12	1.17	1.03	1.09	1.09	1.34	0.8	1.07	1.04
Yb	2.42	2.38	2.46	2.42	2.35	2.33	2.3	2.3	1.99	2.72	2.64
Lu	0.356	0.388	0.353	0.365	0.337	0.318	0.353	0.333	0.278	0.408	0.402
Hf	7.17	7.24	8.09	7.75	7.61	7.56	7.79	7.88	7.72	6.11	7.55
Ta	1.39	1.4	1.62	1.45	1.47	1.41	1.5	1.67	1.21	0.99	1.9
Th	6.05	6.9	12.3	8.42	11.67	11.62	10.82	9.65	8.67	6.07	4.47
Sc	18.7	19.8	20	19.71	18.24	18.22	18.34	17.87	14.45	27.5	14.97
Co	31.5	30.1	27.6	27.8	26.8	27.2	27.9	29.6	23.8	37.6	24.8
<i>Isotopic analyses</i>											
^ε _{Nd}	-9.68	-10.01	-9.73	-10.34	-10.07	-9.81	-	-9.05	-	-11.30	-6.91
⁸⁷ Sr/ ⁸⁶ Sr	0.70708	0.70701	0.70703	0.70709	0.70695	0.70700	-	0.70727	-	0.70723	0.70642

^a Mg number = $[\text{Mg}^{2+} / (\text{Mg}^{2+} + \text{Fe}^{2+})] \times 100$, assuming $\text{Fe}^{2+} = 0.85$ of total Fe.

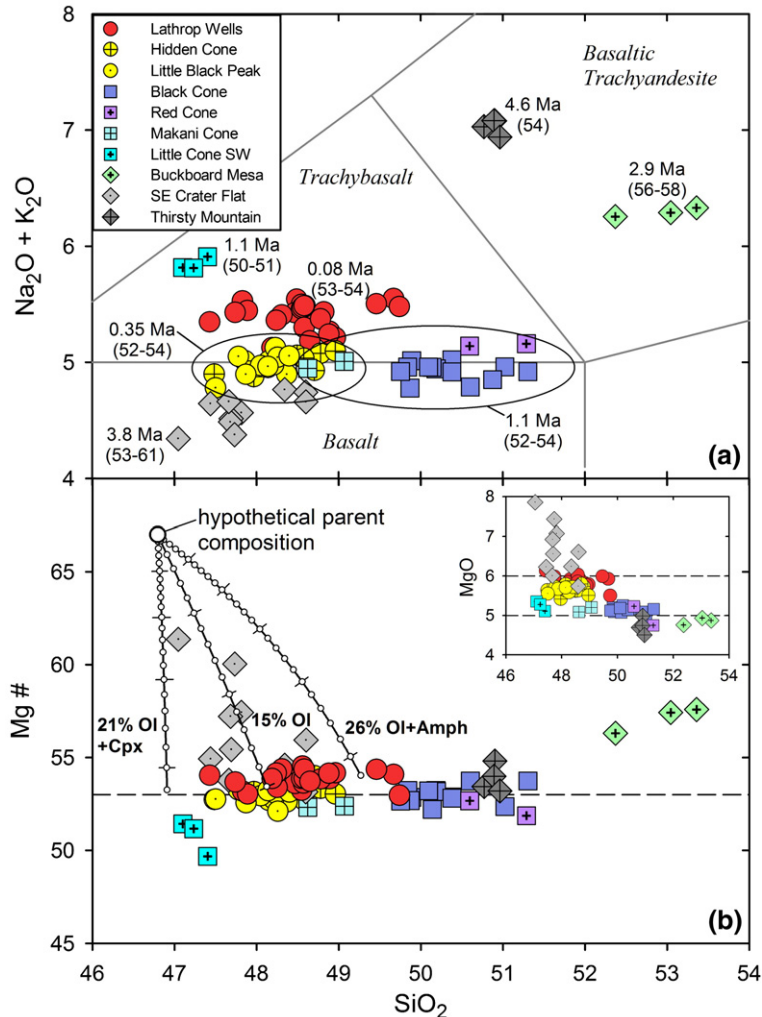


Fig. 4. (a) Total alkalis versus silica for Plio-Pleistocene basalts of the SNVF. Rock classification fields are from Le Bas et al. (1986). Numbers by each episode/compositional group indicate age in Ma. Numbers in parentheses indicate range in Mg number for each group. Compositional diversity at similar Mg numbers suggest compositionally diverse parental magmas. (b) Mg number versus silica for Plio-Pleistocene basalts of the SNVF. Inset is MgO versus silica. Mg number = $[\text{Mg}^{2+}/(\text{Mg}^{2+} + \text{Fe}^{2+})] \times 100$, assuming $\text{Fe}^{2+}/(\text{Fe}^{2+} + \text{Fe}^{3+})$ of magma = 0.85. Dashed reference lines indicate Mg number = 53 and MgO = 5 to 6%. Crystallization curves indicate the type and percentage of minerals fractionated from a parent magma to derive SNVF magmas with Mg numbers of 53–54. Hypothetical parent composition was derived by reverse calculation of olivine fraction (center curve, 15% olivine addition) of a Lathrop Wells trachybasalt (LW22FVP, Table 2) using PETROLOG software (Danyushevsky, 2001). Using the calculated parent composition, assemblages of 50:50 olivine + (clinopyroxene or amphibole) were then subtracted from the parent composition by mass balance calculation. Small circles indicate 1% addition or subtraction of mineral assemblages; tick marks indicate 5% addition or subtraction. Compositions of olivine and clinopyroxene were chosen from PETROLOG results and have Mg numbers of 82; composition of amphibole is that of a phenocryst from Little Cones (Vaniman et al., 1982) and has an Mg number of 69.

which have Mg number and MgO contents as high as 61 and 8%, respectively). This indicates that basalts at each volcano underwent similar degrees of fractional crystallization during ascent (Fig. 4(b)). Plio-Pleistocene basalts characteristically contain olivine as the main phenocryst phase with sparse or no plagioclase phenocrysts. Exceptions are the 3.8 Ma basalt of SE Crater Flat, which also contains phenocrysts of plagioclase and clinopyroxene (Vaniman et al., 1982;

Fleck et al., 1996), the 1.1 Ma basalts of Red Cone and Little Cones, which contain rare amphibole phenocrysts (Vaniman et al., 1982; Bradshaw and Smith, 1994), and the earliest products of the Lathrop Wells volcano (a small component of Lathrop Wells' volume) (Valentine et al., 2007). This observation, combined with trace-element evidence (e.g., high Sr, Table 2) and experimental studies (Mahood and Baker, 1986; Nekvasil et al., 2004) suggests that, for the most part,

fractionation occurred at high pressure (base of the crust or deeper) and involved crystallization of olivine accompanied by clinopyroxene or amphibole, but not plagioclase (Vaniman et al., 1982; Perry and Crowe, 1992; Fleck et al., 1996). Calculation of the amount of fractional crystallization of a parent magma necessary to produce typical Mg numbers of basalts with different SiO₂ contents indicates removal of a crystal assemblage of ~20–25% olivine plus clinopyroxene (or amphibole) and suggests a range of parental magma compositions with SiO₂ contents ranging from ~46–50% (Fig. 4(b)). These results indicate that magmas for each of the

volcanoes had similar fractionation histories during their ascent, with the exception of the SE Crater Flat basalt, which might have undergone some fractionation in a relatively shallow reservoir.

Isotopic data for the basalts also support an interpretation of rapid ascent with little or no crustal residence time or crustal assimilation (Vaniman et al., 1982; Perry and Crowe, 1992; Fleck et al., 1996; Perry et al., 1998). Nd isotopic compositions for all the basalts are nearly uniform across the SNVF and do not vary with SiO₂ content, indicating that magmas did not assimilate SiO₂-rich crustal wallrock (Fig. 5(a)). The Nd isotopic values

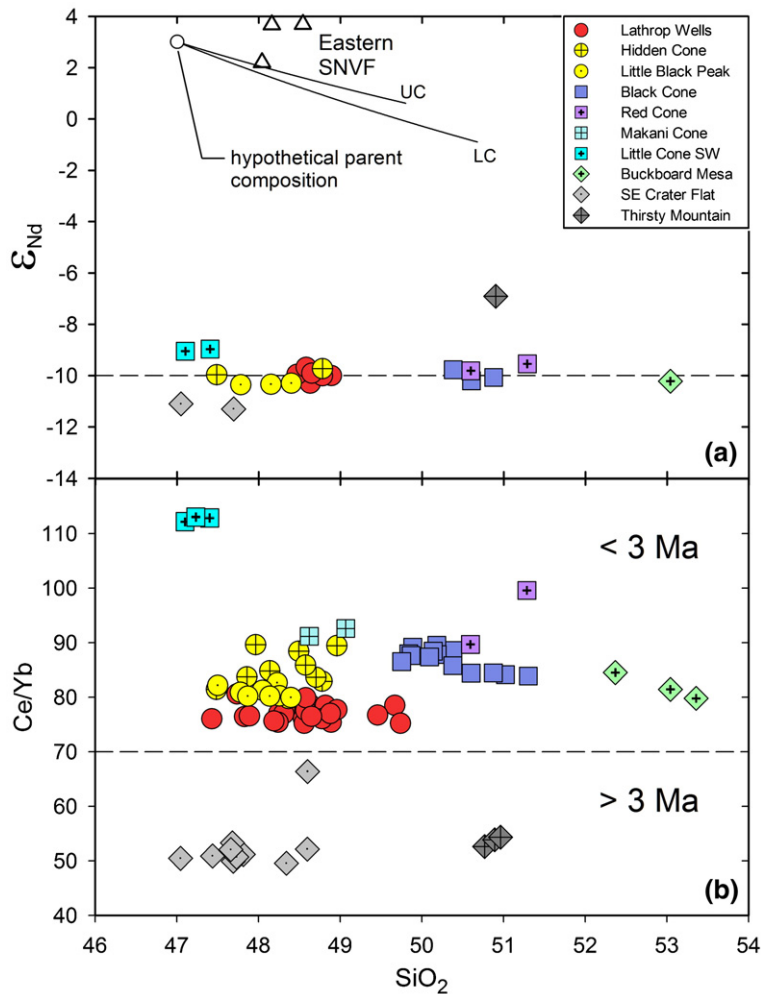


Fig. 5. (a) ϵ_{Nd} versus silica for Plio-Pleistocene basalts of the SNVF. Dashed reference line = ϵ_{Nd} value of -10 . Hypothetical parent composition with $\epsilon_{Nd} = +3$ is based on compositions of basalts from the eastern edge of the SNVF (Farmer et al., 1989), the nearest basalts with “typical” Basin and Range isotopic compositions indicating derivation from an asthenospheric source. Curves labeled LC (lower crust) and UC (upper crust) indicate the compositional changes expected for a magma undergoing high rates of lower and upper crustal contamination. Nd isotopic value for Buckboard Mesa (green diamond) is from Farmer et al. (1989). (b) Ce/Yb versus silica for Plio-Pleistocene basalts of the SNVF. Dashed reference line separates Ce/Yb of basalts older and younger than 3 Ma. Systematic differences in Ce/Yb caused by crustal assimilation, fractional crystallization, or fundamental differences in the mantle source (i.e., asthenosphere versus lithosphere) are ruled out by isotopic or major-element chemistry and instead suggest differences in the degree of partial melting of a heterogeneous lithospheric mantle source.

are unusual in having extremely low $^{143}\text{Nd}/^{144}\text{Nd}$ ratios (corresponding to low ϵ_{Nd} values in the range of -9 to -11) compared to typical alkali basalts of the Basin and Range (Fig. 5(a)). At face value, such low ϵ_{Nd} values could be taken to indicate substantial crustal assimilation during ascent, or extended residence in crustal chambers, of parental magmas. However, an assimilation model would normally assume an initial magma composition with ϵ_{Nd} values typical of Basin and Range basalts derived from an asthenospheric mantle source (Fig. 5(a)). Assuming ϵ_{Nd} values >0 , substantial assimilation of upper and lower crustal rocks results in shifts of only 2–4 ϵ_{Nd} units, far short of the 12–14 unit shifts needed to account for the Nd isotopic compositions of the SNVF basalts (Fig. 5(a)). Vaniman et al. (1982) and Farmer et al. (1989) used similar reasoning and observations on the uniformity of isotopic values across the region to conclude that the Sr and Nd isotopic values of the SNVF are primary characteristics of the mantle source, i.e., that the source is old, lithospheric mantle.

Despite the similarities in degree of fractional crystallization and isotopic composition, basalts of different ages do show systematic differences in incompatible trace-element composition. Basalts younger than 3.8 Ma have substantially higher concentrations of elements such as Sr, La and Th (Vaniman et al., 1982; Farmer et al., 1989). These basalts are also relatively light-rare-earth element enriched, as measured by Ce/Yb (Fig. 5(b)). The lack of correlation between Ce/Yb and SiO_2 for basalts of all ages indicates that higher Ce/Yb values are not due to crustal assimilation or fractional crystallization, or to major differences of the mantle source (i.e., asthenosphere vs. lithospheric mantle). This conclusion is consistent with the narrow range of isotopic compositions of the basalts discussed above. Instead, increased Ce/Yb indicates a decreased amount of partial melting for basalts <3 Ma, a conclusion consistent with the observed decrease in volcano volume with time (Fig. 3). Similarity in degree of fractional crystallization from parental basalts and lack of evidence of crustal assimilation suggests all the basalts younger than 3 Ma followed similar (i.e., rapid) ascent paths through the crust and that differences in eruption volumes can be considered roughly proportional to differences in partial melt volumes in the mantle.

3. Time–volume behavior of Plio-Pleistocene basalts

There are two fundamental types of time–volume relationships for basaltic volcanic fields (Fig. 6). Volume-predictable behavior (Fig. 6(a)) results in a linear relationship (during a period of constant long-term eruptive flux) between the cumulative volume of

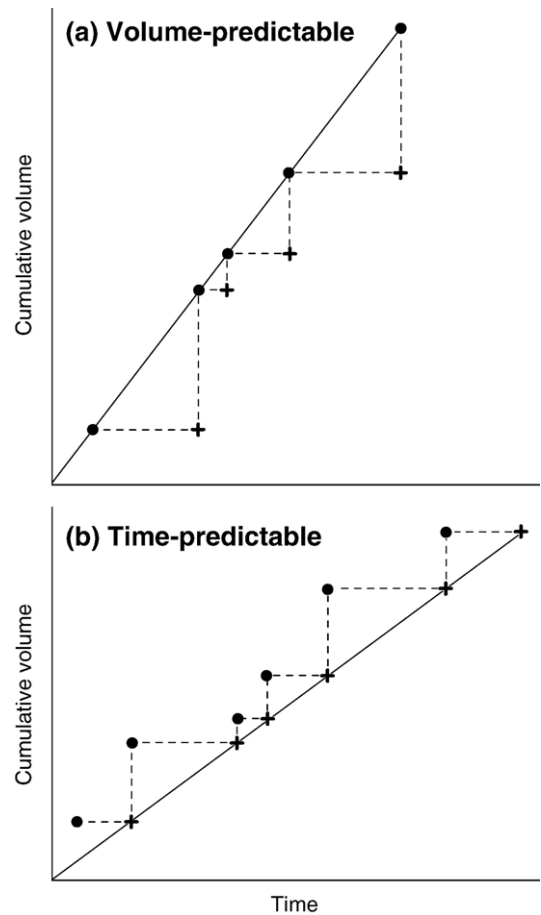


Fig. 6. Illustration of two fundamental types of time–volume relationships for volcanic fields. Filled circles represent the age of an episode and the cumulative volume of that episode and all preceding episodes. Crosses represent the age of an episode and the cumulative volume of preceding episodes only. (a) An illustrative example of volume-predictable behavior. (b) Illustrative example of time-predictable behavior. The slope of the lines in each plot is the eruptive volume flux.

an eruptive episode plus prior episodes and its age or timing. If one has knowledge of the long-term eruptive flux (based upon the geologic record in the volcanic field), then the volume of an episode can be predicted for a given repose period. However, timing of a future episode cannot be forecast based upon the time–volume behavior alone (e.g., Kuntz et al. (1986)). In contrast, time-predictable behavior (Fig. 6(b)) results in a linear relationship between the timing of an episode and the cumulative volume of prior episodes only (assuming a constant long-term eruptive flux). Repose time after an event is proportional to the event’s volume, therefore the timing of a future episode can be forecast with knowledge of preceding volumes. However, the volume of the future episode cannot be forecast based upon the time–volume behavior alone (e.g., Bacon (1982)).

A plot of cumulative volume of Plio-Pleistocene episodes in the SNVF as a function of their ages (Fig. 7 (a)), using volumes corrected for erosion; see Table 1), suggests at first glance that eruptive volume flux decreased after ~ 2.9 Ma but has been relatively steady and volume-predictable since. In detail, though, the system is not volume-predictable. For example, a repose interval of ~ 750 kyr (between the 1.1 Ma and 350 ka episodes) resulted in eruption of ~ 0.11 km³, similar to the volume of the most recent episode after only a ~ 275 kyr repose interval.

A better correlation emerges when the time of each eruptive episode is plotted as a function of cumulative volume from preceding episodes (crosses on Fig. 7(a)). Episodes <3 Ma form a linear, time-predictable relationship, with a slope indicating a constant eruptive

flux of ~ 0.5 km³/Myr. The relationship between time and volume can be formulated as a linear regression model where the interval to the next eruptive episode is dependent on the volume of the previous eruptive episode. The regressed data are the volume and time to the next episode for the 2.9, 1.1, and 350 ka episodes. Volumes for the Quaternary volcanoes are assumed to be the corrected volumes (to account for tephra fallout volume) listed in Table 1 and the time intervals between episodes are 1.8, 0.75, and 0.27 Ma. The regression line is described by the equation, T (to next episode) = $(2.108V) + 0.019$, with $r^2 = 0.999$; the association between time and volume is statistically significant ($P < 0.05$). Using uncorrected volumes, $r^2 = 0.964$ and the association between time and volume is not statistically significant ($P > 0.05$). Episodes older than 2.9 Ma appear to represent a higher eruptive flux, although there are insufficient data to quantify this. As discussed previously (see Fig. 5(b)), Ce/Yb data provide evidence that the decreased degree of partial melting of the mantle source coincides with the timing of the shift to the lower eruptive flux apparent in the time–volume data beginning at 2.9 Ma (Fig. 7(b)).

4. Interpretation

Bacon (1982) suggested that time-predictable behavior in the bimodal Coso volcanic field (California) reflected passive response of magma to a constant strain rate in the extending crust. Dike injection associated with an eruptive episode at Coso relieved accumulated elastic strain in proportion to the episode volume via emplacement of dikes into the shallow crust. Thus a large volume eruptive episode resulted in a long repose interval to the next episode. This model is the starting point for our interpretation of time-predictable behavior in the Southwest Nevada Volcanic Field, which also resides in an extensional tectonic setting. We consider that the recent behavior of the SNVF reflects the response of the lithosphere as a whole (crust and lithospheric mantle) to extensional tectonics.

The presence of a non-convecting lithospheric mantle source beneath the SNVF is key to our model: melt generation and extraction processes are fundamentally different from those in the asthenosphere where melt can be generated by convective upwelling and decompression. A static lithospheric source will favor long-term preservation of compositional and mineralogical heterogeneities that probably originated by influx of arc fluids and hydrous melts during subduction beginning in the Early Proterozoic (Farmer et al., 1989). The presence of small-scale heterogeneities rich in hydrous minerals is

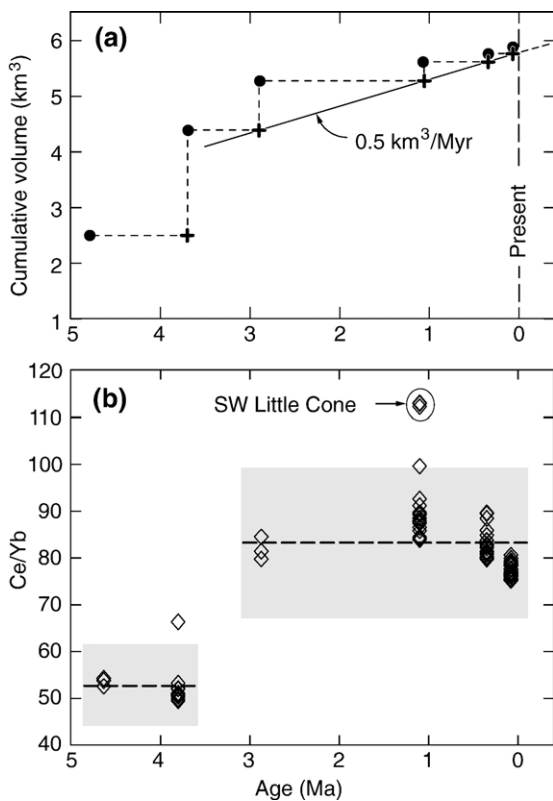


Fig. 7. (a) Plot of volume–age relationships in Plio-Pleistocene basalts of Southwestern Nevada Volcanic Field. Filled circles are cumulative volume versus age of each episode, while crosses show time-predictable trend of cumulative volume just prior to an episode versus age of the episode (b) Ce/Yb versus age for Plio-Pleistocene basalts. The shift to higher but variable Ce/Yb beginning at 2.9 Ma indicates a shift to generally lower degrees of partial melting. SW Little Cone is a very small volcano with nepheline-normative composition, suggesting smaller degree of melting at higher pressure than other basalts in the 1.1 Ma episode. Dashed lines and shaded fields represent the mean and two standard deviations, respectively, for Ce/Yb values of >3 Ma and <3 Ma basalts.

probably a prerequisite for generating and accumulating melt in “cold” lithospheric mantle, and is consistent with small-volume and infrequent eruption of basalt over the past 5 Ma (Gallagher and Hawkesworth, 1992; Harry and Leeman, 1995). High water contents in olivine melt inclusions from Pleistocene basalts (up to 3.5 wt.% [(Nicholis and Rutherford, 2004)]) and rare amphibole phenocrysts (Vaniman et al., 1982; Bradshaw and Smith, 1994) provide evidence of hydrous melting, consistent with the notion of mantle heterogeneities that are inherited from previous influx of volatile- and incompatible element-rich fluids. Zones of hydrous lithospheric mantle containing small melt fractions are rheologically weaker than surrounding mantle and deform more readily under extensional strain. Deformation of these zones increases porosity, resulting in enhanced melt migration toward the zones and the formation of melt bands that further enhance melt migration and shear localization (Katz et al., 2006; Schmeling, 2006). Enhanced shear along melt bands can accommodate small amounts of extensional strain by minor lithospheric thinning at depth. As melt is focused into localized pockets or bands, buoyancy forces and magma pressure increase until they reach a critical value that results in upward propagation of dikes. The critical pressure is determined by horizontal tectonic stresses and rock properties; therefore the triggering of dikes and the resulting volcanic episodes are determined by the response of the heterogeneous mantle to regional tectonics. This “passive” process of melt collection and dike initiation in response to tectonic strain is consistent with time-predictable behavior of the system, with the extension rate and volume of mantle involved in melt accumulation (which is partially a function of the scale of heterogeneities) determining the volume and timing of an episode at source depths.

Data on volume, eruptive fissure length, and estimated effusion rate further support the argument that volcanism is closely linked to tectonic strain in the crust, in addition to the mantle processes described above. In Section 2.2 we suggested that the fissure length is related to the feeder dike length at depth, which in turn is closely related to the length scale of the mantle source that is tapped to feed each volcano. Fissure length of the 2.9 Ma episode was ~2.5 km (Fig. 3). In simple elastic media the width (w) to length (l) ratios of dikes are related to driving pressure and elastic properties of the country rock as

$$\frac{w}{l} \propto \frac{P_d}{\mu/(1-\nu)}, \quad (1)$$

where P_d is the driving pressure (the difference between magma pressure in the dike and the horizontal stress in the

country rocks), μ is the elastic shear modulus, and ν is Poisson’s ratio (Pollard, 1987). If we assume that the ≤ 2.9 Ma episodes were driven by dikes with similar P_d (consistent with relatively constant tectonic stresses) through lithospheric sections with similar elastic properties, then longer feeder dikes and fissures imply proportionally wider dikes. Therefore the 2.9 Ma episode would have locally relieved 2.5–5 times more horizontal elastic strain than the 1.1 Ma episode which consisted of five separate small volcanoes that each had fissures on average ~0.5–1 km long and volumes roughly an order of magnitude smaller than the 2.9 Ma episode. Accordingly, repose after the 2.9 Ma episode was ~1.8 Myr, while the smaller 1.1 Ma episode was followed by a repose period of ~750 kyr.

The variation in effusion rates of individual volcanoes (Fig. 3) is consistent with the above interpretation. The inferred lava effusion rate of ~100 m³/s during the 2.9 Ma episode was ~25–500 times larger than those of the ≤ 1.1 Ma volcanoes (Valentine and Perry, 2006). At depths below which significant vesiculation has occurred, the volumetric flux of magma (Q) between parallel-sided dike walls probably follows the Poiseuille relationship where

$$Q \propto l \frac{w^3}{\eta} \frac{\partial P}{\partial z} \quad (2)$$

(η is magma viscosity, P is magma pressure, and z is vertical distance (Bird et al., 1960)). Assuming similar magma viscosities and pressures for the eruptive episodes, we have $Q \propto lw^3$. The 2.9 Ma episode would then be expected to have effusion rates >40 times higher than those estimated for the ≤ 1.1 Ma episodes, consistent with the effusion rates inferred from field data. This corroborates the occurrence of wider dikes associated with longer fissures and larger eruptive volumes of events, and similar magma pressures that trigger dikes. In detail the driving pressures and elastic properties of country rocks must have varied to some degree, along with other factors that affect magma discharge (e.g., volatile content); nevertheless, the simple estimates above show that the time-predictable behavior is consistent to first order with several properties of the Plio-Pleistocene volcanoes within a context where the average volumetric eruption rate is directly related to localized response to regional tectonic strain rate.

Location and orientation of successive episodes might also be related to elastic strain relief by occasional dike injection. Basaltic episodes occurred in different parts of the Plio-Pleistocene SNVF with episodes focused in the northern part (at 4.6 Ma, 2.9 Ma, and 350 ka) alternating with episodes in the southern part (3.8 Ma, 1.1 Ma, and

77 ka). We suggest that the limited N–S extent of an episode meant that strain relief in the dominantly E–W extensional setting (minimum horizontal principal stress, σ_3 , has been oriented $\sim N60^\circ W$ in Plio-Pleistocene times (Fleck et al., 1996)) was not evenly distributed after the episode. Therefore the largest amount of stored elastic strain for the subsequent episode to accommodate would be toward the opposite side (in the N–S direction) of the field, resulting in a pattern of eruption episodes alternating between the northern and southern parts of the field. The volcanoes of the 1.1 Ma and 350 ka episodes, along with the 3.8 Ma anomalies G, F, and H, are aligned roughly perpendicular to σ_3 . Each volcano in these episodes probably represents an individual source-to-surface dike event, but we propose that the alignments might represent progressive collection of melt along bands within the lithospheric mantle as it responds to regional stress by deformation (see discussion above and Katz et al. (2006)), where the melt band orientation is perpendicular to σ_3 . At very shallow depths (i.e., 100s of m), however, each dike event was captured by older N–S trending normal faults (Connor et al., 2000; Valentine and Krogh, 2006; Perry et al., 2006; Valentine and Keating, in press).

In summary, our interpretation has the following main elements. The lithospheric mantle beneath the SNVF is mineralogically and compositionally heterogeneous, resulting in small fractions of melt that reside in pockets that respond to slow, steady extension by shear deformation and localized porosity increase. The shearing and porosity increase, in turn, further focuses melt into the pockets or bands. As melt focuses into pockets, fluid pressure builds due to buoyancy until a sufficient overpressure is attained to initiate and drive dikes upward. Magma is transported toward the surface relatively rapidly via dike(s); the resulting dike(s) add mass to the lithosphere above the melt source and relieves elastic strain. Tectonic strain relief at the depth of the melt sources takes place primarily through slow shearing and thinning of the lithospheric mantle, but at higher levels the elastic (tectonic) strain relief occurs quickly upon dike injection. This model is consistent with the physical volcanology, geochemistry, and time–volume history of the SNVF during the past 2.9 Myr.

5. Implications

5.1. Tectonically and magmatically controlled basaltic fields

We suggest that there are two end member types of continental basaltic fields that relate the properties of

time- and volume-predictability, and interaction with shallow structure. The first type, which we term a *tectonically controlled* field, is exemplified by basaltic volcanism in the Southwestern Nevada Volcanic Field during the past 2.9 Myr. In tectonically controlled fields, magma flux is very low and is a passive byproduct of regional tectonic strain. If the underlying mantle has heterogeneities in the form of locally hydrous and/or partially molten zones, melt will concentrate in these localized zones and magma pressure can occasionally build to sufficient levels to propagate dikes through the crust and feed eruptions. Dike lengths are determined primarily by the volume of the magmatic event, which is related to the length scale of mantle compositional heterogeneity that feeds the event. Dike emplacement relieves local stresses that must rebuild over a period of time that is proportional to the volume of the event. Because of the low rate of dike injection in tectonically controlled fields, strain in the shallow crust is mainly taken up by faulting. Most dikes that ascend into the faulted shallow crust are likely to be captured by those faults and therefore might have near-surface dike orientations and coeval vent alignments that are not simply perpendicular to the least principal stress (i.e., if fault orientations are inherited from past stress fields; Valentine and Krogh, 2006; Perry et al., 2006; Valentine and Keating, in press). The connection between the regional tectonic strain and magma transport (Bacon, 1982) means that a tectonically controlled field is likely to exhibit time-predictable behavior. In tectonically controlled fields, melt generation is dependent on tectonic forces, otherwise melt would not be able to accumulate and ascend.

The second end member of volcanic fields is *magmatically controlled*, and is characterized by relatively high magma fluxes. Frequent dike injection equals or exceeds regional tectonic strain and faulting is relatively rare (Parsons and Thompson, 1991; Kuntz et al., 2002). As a result, dikes are not captured by pre-existing faults as they near the surface, and their orientations (as reflected by, for example, alignments of coeval vents or fissures) are generally perpendicular to the regional least principal stress. The volume of an eruptive episode depends upon the magma flux and the repose time since the previous eruption, i.e., they are volume-predictable. Eruptions in magmatically controlled fields occur as pressures build up in magma reservoirs, driven primarily by processes such as melt accumulation, fractionation, and concentration of volatiles. An excellent example is the eastern Snake River Plain (Fig. 1). Note the difference in estimated long-term eruptive fluxes: the tectonically controlled SNVF has an estimated flux of

0.5 km³/Myr during the past 2.9 Myr (among the lowest of any basaltic field on Earth (Perry et al., 1998)), while estimated fluxes in the Great Rift area of the ESRP range between 500–2500 km³/Myr (based primarily upon the Holocene record (Kuntz et al., 1986)). Melt generation in magmatically controlled fields is due to thermal structure of the mantle and is not dependent upon tectonics.

5.2. Implications for volcanic risk assessment

Urbanization and construction of long-term facilities in basaltic fields creates an important class of volcanic risk assessment problems. Estimation of event probabilities in basaltic fields that are dominated by monogenetic volcanoes requires forecasts of both the recurrence rates (or timing) and locations of future events. If basaltic volcanism in the SNVF continues to exhibit tectonically controlled, time-predictable behavior with a ~0.5 km³/Myr eruptive volume flux, the linear regression model (time to next episode is dependent on previous episode's volume) suggests that the next episode of volcanic activity somewhere in the volcanic field will occur about 270 kyr after the Lathrop Wells episode (with a 90% prediction interval of ±290 kyr reflecting the small data set), or about 190 kyr in the future. The interval to the next episode predicted by the time–volume relationship is consistent with SNVF recurrence intervals that have been estimated using probabilistic approaches (Crowe, 1986; Perry et al., 1998; Connor et al., 2000). One caveat is that it is possible that the ~77 ka eruption of Lathrop Wells volcano might be the beginning of an episode rather than comprising an entire episode. The lapsed time since the Lathrop Wells event suggests that it is likely to have been the lone event in its episode, although this cannot be proven. This highlights the value of probabilistic approaches that incorporate uncertainties into temporal (recurrence) models, rather than relying only on the more deterministic, empirical time-predictable behavior. Additionally, time-predictability in a tectonically controlled field does not, by itself, constrain the location or size of potential future episodes, requiring the incorporation of additional information. We have shown in previous papers that volcano location in the low-flux SNVF depends primarily upon the location and areal extent of the mantle source that is tapped (magma footprint (Valentine and Perry, 2006)), and secondarily upon shallow structure and surface topography (Valentine and Krogh, 2006; Gaffney and Damjanac, 2006). The fact that most of the basaltic episodes (except the ~2.9 Ma Buckboard Mesa event) have returned to the vicinity of existing clusters (Connor et al., 2000) suggests that the magmatic footprints of future events will probably also occur near or within those

clusters. Likewise, general similarities in volcano size and eruptive styles during the past ~1.1 Myr (Table 1) suggest that the future events during the next 100s of kyr will have similar characteristics. All of these factors form potentially important aspects of probabilistic risk assessment in the SNVF, where the proposed Yucca Mountain radioactive waste repository is sited, and they should come into play in risk assessments in other volcanic fields.

Acknowledgements

Discussions with Bob Youngs and Karen Jenni improved our statistical approach. We thank R.E. Kelley and Tom McTighe for GIS support, and A. Kron for graphics support. D. Krier, D. Vaniman, D. Hickmott, E. Smistad, P. Swift, K. Coppersmith, and E. Gaffney, H.-U. Schmincke, and an anonymous reviewer provided very useful reviews. This work is funded by the U.S. Department of Energy's Yucca Mountain Project.

References

- Aranda-Gómez, J.J., Luhr, J.F., Housh, T.B., Connor, C.B., Becker, T., Henry, C.D., 2003. Synextensional Pliocene–Pleistocene eruptive activity in the Camargo volcanic field, Chihuahua, México. *Geol. Soc. Amer. Bull.* 115, 289–313.
- Bacon, C.R., 1982. Time-predictable bimodal volcanism in the Coso Range, California. *Geology* 10, 65–69.
- Bird, R.B., Steward, W.E., Lightfoot, E.N., 1960. *Transport Phenomena*. Wiley, New York.
- Bradshaw, T.K., Smith, E.I., 1994. Polygenetic Quaternary volcanism at Crater Flat, Nevada. *J. Volcanol. Geotherm. Res.* 63, 165–182.
- Briggs, R.M., Okada, T., Itaya, T., Shibuya, H., Smith, I.E.M., 1994. K–Ar ages, paleomagnetism, and geochemistry of the south Auckland volcanic field, North Island, New Zealand, New Zeal. *J. Geol. Geophys.* 37, 143–153.
- Camp, V.E., Roobol, M.J., Hooper, P.R., 1991. The Arabian continental alkali basalt province: Part II. Evolution of Harrats Khaybar, Ithnayn, and Kura, Kingdom of Saudi Arabia. *Geol. Soc. Amer. Bull.* 103, 363–391.
- Cande, S.C., Kent, D.V., 1995. Revised calibration of the geomagnetic polarity time scale for the Late Cretaceous and Cenozoic. *J. Geophys. Res.* 100, 6093–6095.
- Condit, C.D., Crumpler, L.S., Aubele, J.C., Elston, W.E., 1989. Patterns of volcanism along the southern margin of the Colorado Plateau: the Springerville field. *J. Geophys. Res.* 94, 7975–7986.
- Connor, C.B., 1990. Cinder cone clustering in the TransMexican Volcanic Belt: implications for structural and petrologic models. *J. Geophys. Res.* 95, 19395–19405.
- Connor, C.B., Stamatakos, J.A., Ferrill, D.A., Hill, B.E., Ofoegbu, G.I., Conway, F.M., Sagar, B., Trapp, J., 2000. Geologic factors controlling patterns of small-volume basaltic volcanism: application to a volcanic hazards assessment at Yucca Mountain, Nevada. *J. Geophys. Res.* 105, 417–432.
- Crowe, B.M., 1986. Volcanic hazard assessment for disposal of high-level radioactive waste. *Active Tectonics*. National Academy Press, Washington, DC, pp. 247–260.

- Danyushevsky, L.V., 2001. The effects of small amounts of H₂O on the crystallization on mid-ocean ridge and backarc basin magmas. *J. Volcanol. Geotherm. Res.* 110, 265–280.
- DePaolo, D.J., Daley, E.E., 2000. Neodymium isotopes in basalts in the southwest basin and range and lithospheric thinning during continental extension. *Chem. Geol.* 169, 157–185.
- Farmer, G.L., Perry, F.V., Semken, S., Crowe, B., Curtis, D., DePaolo, D.J., 1989. Isotopic evidence on the structure and origin of subcontinental lithospheric mantle in southern Nevada. *J. Geophys. Res.* 94, 7885–7898.
- Fleck, R.J., Turrin, B.D., Sawyer, D.A., Warren, R.G., Champion, D.E., Hudson, M.R., Minor, S.A., 1996. Age and character of basaltic rocks of the Yucca Mountain region, southern Nevada. *J. Geophys. Res.* 101, 8205–8227.
- Fridrich, C.J., Whitney, J.W., Hudson, M.R., Crowe, B.M., 1999. Space-time patterns of Late-Cenozoic extension, vertical axis rotation, and volcanism in the Crater Flat basin, southwest Nevada. *Spec. Pap. Geol. Soc. Am.* 333, 197–212.
- Gaffney, E.S., Damjanac, B., 2006. Localization of volcanic activity: topographic effects on dike propagation, eruption, and conduit formation. *Geophys. Res. Lett.* 33, L14313, doi:10.1029/2006GL026852.
- Gallagher, K., Hawkesworth, C., 1992. Dehydration melting and the generation of continental flood basalts. *Nature* 358, 57–59.
- Harry, D.L., Leeman, W.P., 1995. Partial melting of melt metasomatized subcontinental mantle and the magma source potential of the lower lithosphere. *J. Geophys. Res.* 100, 10255–10269.
- Heizler, M.T., Perry, F.V., Crowe, B.M., Peters, L., Appelt, R., 1999. The age of the Lathrop Wells volcanic center: an ⁴⁰Ar/³⁹Ar dating investigation. *J. Geophys. Res.* 104, 767–804.
- Katz, R.F., Spiegelman, M., Holtzman, B., 2006. The dynamics of melt and shear localization in partially molten aggregates. *Nature* 442, 676–679.
- Keating, G.N., Valentine, G.A., Krier, D.J., Perry, F.V. in press. Shallow plumbing systems for small-volume basaltic volcanoes, *Bull. Volcanol.* doi:10.1007/s00445-007-0154-1.
- Kuntz, M.A., Champion, D.E., Spiker, E.C., Lefebvre, R.H., 1986. Contrasting magma types and steady-state, volume-predictable, basaltic volcanism along the Great Rift, Idaho. *Geol. Soc. Amer. Bull.* 97, 579–594.
- Kuntz, M.A., Anderson, S.R., Champion, D.E., Lanphere, M.A., Grunwald, D.J., 2002. Tension cracks, eruptive fissures, dikes, and faults related to Late Pleistocene–Holocene basaltic volcanism and implications for the distribution of hydraulic conductivity in the eastern Snake River Plain, Idaho. *Spec. Pap. Geol. Soc. Am.* 353, 111–133.
- Le Bas, M.J., Le Maitre, R.W., Streckeisen, A., Zanettin, B.A., 1986. Chemical classification of volcanic rocks based on the total alkali–silica diagram. *J. Petrol.* 27, 745–750.
- Leeman, W.P., Harry, D.L., 1993. A binary source model for extension-related magmatism in the Great Basin. *Science* 262, 1550–1554.
- Livaccari, R.F., Perry, F.V., 1993. Isotopic evidence for preservation of Cordilleran lithospheric mantle during the Sevier–Laramide orogeny, western United States. *Geology* 21, 719–722.
- Mahood, G.A., Baker, D.R., 1986. Experimental constraints on depths of fractionation of mildly alkalic basalts and associated felsic rocks: Pantelleria, Strait of Sicily. *Contrib. Mineral. Petrol.* 93, 251–264.
- Nekvasil, H., Dondolini, A., Horn, J., Filiberto, J., Long, H., Lindsley, D.H., 2004. The origin and evolution of silica-saturated alkalic suites: an experimental study. *J. Petrol.* 45, 693–721.
- Nicholis, M.G., Rutherford, M.J., 2004. Experimental constraints on magma ascent rate for the Crater Flat volcanic zone hawaiiite. *Geology* 32, 489–492.
- Parsons, T., Thompson, G.A., 1991. The role of magma overpressure in suppressing earthquakes and topography: worldwide examples. *Science* 253, 1399–1402.
- Perry, F.V., Crowe, B.M., 1992. Geochemical evidence for waning magmatism and polycyclic volcanism at Crater Flat, Nevada. *Proceedings High-Level Radioactive Waste Management Conference.* American Nuclear Society, La Grange Park, Illinois, pp. 2356–2365.
- Perry, F.V., Straub, K.T., 1996. Geochemistry of the Lathrop Wells volcanic center. Los Alamos National Laboratory Report LA-13113-MS. 106 pp.
- Perry, F.V., Baldrige, W.S., DePaolo, D.J., 1987. Role of asthenosphere and lithosphere in the genesis of Late Cenozoic basaltic rocks from the Rio Grande rift and adjacent regions of the southwestern United States. *J. Geophys. Res.* 92, 9193–9213.
- Perry, F.V., Baldrige, W.S., DePaolo, D.J., 1988. Chemical and isotopic evidence for lithospheric thinning beneath the Rio Grande rift. *Nature* 332, 432–434.
- Perry, F.V., DePaolo, D.J., Baldrige, W.S., 1993. Neodymium isotopic evidence for decreasing crustal contributions to Cenozoic ignimbrites of the western United States: implications for the thermal evolution of the Cordilleran crust. *Geol. Soc. Amer. Bull.* 105, 872–882.
- Perry, F.V., Crowe, B.M., Valentine, G.A., Bowker, L.M., 1998. Volcanism studies: final report for the Yucca Mountain Project. Los Alamos National Laboratory Report LA-13478-MS. 554 pp.
- Perry, F.V., Cogbill, A.H., Kelley, R.E., 2005. Uncovering buried volcanoes at Yucca Mountain: new data for volcanic hazard assessment. *Eos, Trans. Am. Geophys. Union* 86, 485–488.
- Perry, F.V., Valentine, G.A., Cogbill, A.H., Keating, G.N., Gaffney, E.S., Damjanac, B., 2006. Control of basaltic feeder dike orientation by fault capture near Yucca Mountain, USA. *American Geophysical Union Fall Meeting, San Francisco, 2006, abstract V11B-0572.*
- Pollard, D.D., 1987. Elementary fracture mechanics applied to the structural interpretation of dykes, In: Halls, H.C., Fahrig, W.H. (Eds.), *Mafic Dyke Swarms.* *Geol. Assoc. Can. Spec. Pap.*, vol. 34, pp. 5–24.
- Sawyer, D.A., Fleck, R.J., Lanphere, M.A., Warren, R.G., Broxton, D.E., Hudson, M.R., 1994. Episodic caldera volcanism in the Miocene southwestern Nevada volcanic field: Revised stratigraphic framework, ⁴⁰Ar/³⁹Ar geochronology, and implications for magmatism and extension. *Geol. Soc. Amer. Bull.* 106, 1304–1318.
- Schmeling, H., 2006. A model of episodic melt extraction for plumes. *J. Geophys. Res.* 111, B03202.
- Sonder, L.J., Jones, C.H., 1999. Western United States extension: how the west was widened. *Annu. Rev. Earth Planet. Sci.* 27, 417–462.
- Sudo, M., Uto, K., Tatsumi, Y., Matsui, K., 1998. K–Ar geochronology of a Quaternary monogenetic volcano group in Ojika Jima District, Southwest Japan. *Bull. Volcanol.* 60, 171–186.
- Valentine, G.A., Keating, G.N. in press. Eruptive styles and inferences about plumbing systems at Hidden Cone and Little Black Peak scoria cone volcanoes (Nevada, U.S.A.), *Bull. Volcanol.* in press. doi:10.1007/s00445-007-0123-8.
- Valentine, G.A., Krogh, K.E.C., 2006. Emplacement of shallow dikes and sills beneath a small basaltic volcanic center — the role of pre-existing structure (Paiute Ridge, southern Nevada, USA). *Earth Planet. Sci. Lett.* 246, 217–230.
- Valentine, G.A., Perry, F.V., 2006. Decreasing magmatic footprints of individual volcanoes in a waning basaltic field. *Geophys. Res. Lett.* 33, L14305, doi:10.1029/2006GL026743.
- Valentine, G.A., Perry, F.V., Krier, D., Keating, G.N., Kelley, R.E., Cogbill, A.H., 2006. Small-volume basaltic volcanoes: eruptive products and processes, and post-eruptive geomorphic evolution in

- Crater Flat (Pleistocene), southern Nevada. *Geol. Soc. Amer. Bull.* 118, 1313–1330.
- Valentine, G.A., Krier, D.J., Perry, F.V., Heiken, G., 2007. Eruptive and geomorphic processes at the Lathrop Wells scoria cone volcano. *J. Volcanol. Geotherm. Res.* 161, 57–80.
- Vaniman, D.T., Crowe, B.M., Gladney, E.S., 1982. Petrology and geochemistry of hawaiite lavas from Crater Flat, Nevada. *Contrib. Mineral. Petrol.* 80, 341–357.
- Wahl, R.R., Sawyer, D.A., Minor, S.A., Carr, M.D., Cole, J.C., Swadley, W.C., Laczniak, R.J., Warren, R.G., Green, K.S., Engle, C.M., 1997. Digital geologic map database of the Nevada Test Site area, Nevada, U.S. Geol. Surv. Open File Rep. 97–140.
- Walker, G.P.L., 1973. Lengths of lava flows. *Philos. Trans. R. Soc. Lond., A* 274, 107–118.